JOURNAL OF AIRCRAFT
Vol. 45, No. 5, September–October 2008

Design of a High-Lift, Thick Airfoil for Unmanned Aerial Vehicle Applications

David F. Cerra* and Joseph Katz†
San Diego State University, San Diego, California 92182

DOI: 10.2514/1.36924

The aerodynamic design of high-altitude unmanned aerial vehicles is driven by the rapidly decreasing air density at the upper boundaries of the atmosphere. A corresponding increase in wing area cannot provide a simple solution because of the additional weight and flexibility of the high-aspect-ratio wings. The excessive spanwise flexibility can be addressed by developing thicker airfoil sections that will increase the wing bending stiffness. Additional reduction in the expected wing size could be achieved by increasing the design cruise lift coefficient. Consequently, the objective of this study was to develop a 24% thick, two-element airfoil section capable of lift coefficients approaching two. Expected operational Reynolds number was estimated within the range of 0.5 to 1.0 × 10^6. A secondary objective of this study was to experiment with the airfoil design-optimization procedure, which later could be automated.

Nomenclature

A_1	=	constant in Eq. (1)
C_d	=	drag coefficient
C_L	=	wing lift coefficient
C_l	=	airfoil section lift coefficient
C_p	=	pressure coefficient
c	=	chord
D	=	drag
L	=	lift
M	=	Mach number
Re	=	Reynolds number
x	=	chordwise coordinate
α	=	angle of attack
δ	=	flap angle
ρ	=	air density

Introduction

UNMANNED robotic airplanes could provide a less expensive and easily serviceable alternative to communication and surveillance satellites. Solar energy [1,2] could provide the solution for long-term power supply, whereas high-altitude operation is important in terms of reducing atmospheric disturbances and increasing sensors' view angle. However, with increasing altitude, the rapid change in air density requires very large lifting surfaces. To demonstrate this effect of high-altitude flight, consider a simple low-speed case and assume a Mach number of $M = 0.3$ (to be able to overcome high-altitude currents for station keeping) and a moderate takeoff lift coefficient of $C_L = 0.4$, because, clearly, a large wing area is needed. For simplicity, a fixed weight and solar propulsion is assumed (so that fuel mass is not diminishing). The variation of the standard-atmosphere air density vs altitude is plotted in Fig. 1, and here ρ_0 is the density at sea level. If the planned operation altitude is at least 70,000 ft (21,336 m), then, based on this figure, the air density at this altitude drops close to 5% of its sea level value. Assuming all variables are unchanged, then the required lift coefficient will increase according to the hypothetical graph of C_L in Fig. 1. If the airplane in this design is capable of reaching a $C_L = 2.0$, then, still, it cannot climb beyond an estimated altitude of 15 km. To demonstrate how unrealistic the lift requirement may be at the higher altitudes, the "hypothetical C_L" curve was extended to the 70,000 ft altitude in Fig. 1. Therefore, the general conclusion is that, at high altitude, higher lift coefficients and larger wings are needed, combined with the lowest possible structural weight (and higher speed if additional power is available). The low-drag requirement implies the use of high-aspect-ratio wings (to reduce induced drag), which tend to be flexible and structurally unstable. Therefore, increasing the airfoil thickness ratio can clearly increase stiffness and reduce sensitivity to root-bending moments, and result in lighter structural weight. Furthermore, various payloads and fuel can be stored inside a thick wing, contributing to improved overall vehicle efficiency.

Earlier thick airfoil developments [3,4] were not focused directly on unmanned aerial vehicle (UAV) applications, and thickness ratios were near 17% with moderate lift coefficients. More specific efforts to develop airfoils for UAVs [5–9] resulted in higher lift and thicker airfoil designs. Also, small trailing-edge flaps were used, mainly to increase the lift, but flap size was kept small to allow larger volume (for fuel) inside the thick wing. This effort led to airfoils with close to 21% thickness ratio (including the flap) and maximum lift coefficients of over 2.0 (but for Reynolds numbers higher than 2.0×10^6). One of the thickest airfoils tested [10] was developed for the root section of a wind turbine blade. This 24% thick section, however, was not intended for high lift and low drag (and maximum C_L was near 1.3).

The objective of this study is to develop an airfoil of about 24% thickness ratio, capable of a lift coefficient near 2.0, for a Reynolds number range of 0.5 to 1.0×10^6. Because of the high-lift requirement, a two-element airfoil was selected, but with a relatively small trailing-edge flap.

Methodology

The approach used for the airfoil development is described schematically in Fig. 2. Based on the expected Reynolds number range, a generic envelope for the maximum upper surface suction distribution is identified (from [11,12]). These simplified boundaries evolved from the rationale that flow separation is triggered by a steep adverse pressure gradient at the aft section of the airfoil. At the front of the airfoil, however, a near constant, but slightly positive (pressure) gradient is desirable. With this initial generic target, the airfoil shape is modified until the calculated pressure distribution approaches this targeted (pressure distribution) envelope. Liebeck [11,12] provides numerous examples for such pressure distributions and two are shown schematically (by the broken line) in Fig. 2. Note

Presented as Paper 0292 at the 46th AIAA Aerospace Sciences Meeting, Reno, NV, 7–10 January 2008; received 30 January 2008; revision received 5 May 2008; accepted for publication 6 May 2008.

*Graduate Student, Department of Aerospace Engineering and Engineering Mechanics. Member AIAA.
†Professor and Department Chairperson, Department of Aerospace Engineering and Engineering Mechanics. Associate Fellow AIAA.

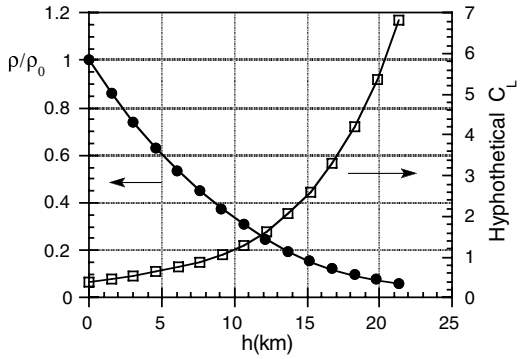

Fig. 1 Variation of relative density ρ/ρ_0 and a hypothetical lift coefficient with altitude h.

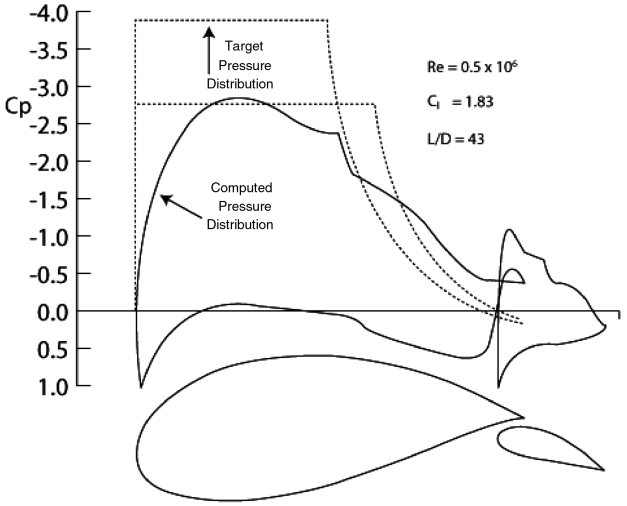

Fig. 2 Schematics of the design strategy: dashed lines show the target and solid lines the calculated pressure coefficients.

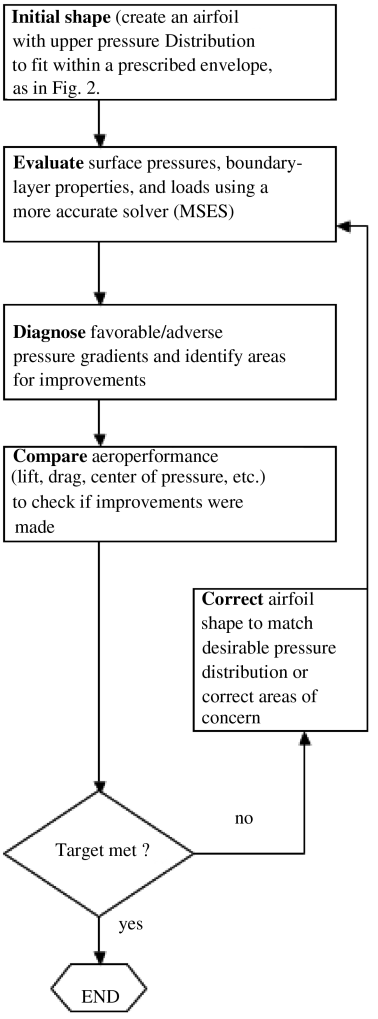

Fig. 3 Flowchart describing the process of configuration development.

that not all prescribed pressure distributions can result in a closed airfoil shape. Therefore, the decision on the convergence of the iterative process is more subjective.

When using ideal flow models (e.g., potential flow), inverse tools [11–13] can be used to provide the desirable airfoil shape based on the shape of the target pressure distribution. However, a more careful examination of the flow, taking into account boundary-layer properties (e.g., friction coefficient, transition, etc.) requires a more advanced computational tool (as in [14]), which also has the two-element airfoil capability, but does not have such an inverse option. Therefore, a possible design iteration sequence may use the inverse mode of the ideal flow solver on each element and verify performance with the more accurate viscous flow solver [14].

It is also important to understand the meaning of the boundaries set by the broken line in Fig. 2. For example, if a favorable pressure gradient exists, then, in general, the boundary layer stays laminar and transition to turbulent flow is delayed. This means that by controlling the slope on the "rooftop" ($x/c < 0.6$ in Fig. 2) we can prescribe the expected transition point. The adverse pressure range ($x/c > 0.6$ in Fig. 2) will trigger transition and, if too steep, flow separation will result. The same considerations can then be applied to the flap, and some specific considerations used in this area will be discussed later. Also note that the adverse pressure envelopes taken from [11] are for single-element airfoils. When a second element is placed behind the main airfoil, larger trailing-edge suction levels can be achieved (carryover). Consequently, for the initial iterations, the adverse pressure gradient (of the broken lines) is used and not the absolute value of the pressure coefficient.

This general design process is summarized schematically in the block diagram of Fig. 3. The process starts with an existing airfoil shape that was gradually modified to fit within the boundaries described in Fig. 2 (excluding the main element trailing edge, where only the target C_P slope was used). At this phase, inverse methods (as in [11,12]) can be used for a rapid definition of the initial airfoil shape, as shown at the bottom of Fig. 2. The design strategy therefore focuses on modifying the upper surface pressure distribution to meet the target lift, whereas the lower surface shape is developed next, mainly to satisfy the thickness requirements. The next level is a more careful examination of boundary-layer properties with more attention to parameters, such as lift and drag. Therefore, a more advanced method is used (such as in [14]), to calculate boundary-layer transition and flow separation, if present (for a range of flap and main element angles of attack). The following blocks in Fig. 3 (marked "Diagnose" and "Compare") represent this process when the computed and target pressure distributions are compared, and areas for improvement are identified. At the same time, the integral results are evaluated, as well, by creating a "performance map" for the range of expected angles of attack. Note that not all improvements in the shape of the pressure distribution lead to improved performance in terms of lift and drag (e.g., the process is not linear). Some examples for the previously described iterative process are provided in the following section.

Development of the Airfoil Shape

The secondary objective of this study is to develop the rationale for the design optimization, which then could be automated. As noted earlier, an arbitrary optimization may not converge to an absolute optimum because of the complexity of the problem. To demonstrate this notion, the effect of small changes in several areas on the airfoil

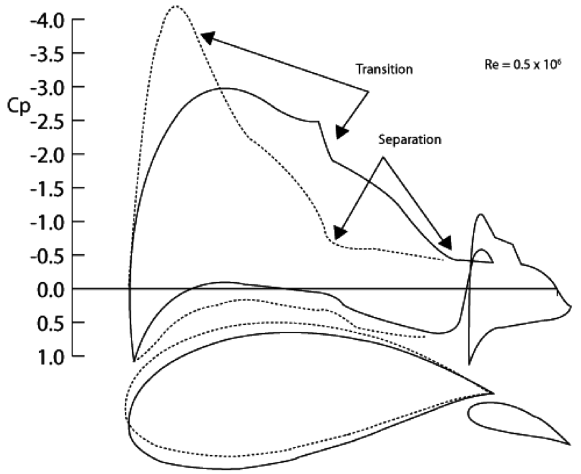

Fig. 4 Effect of changing the leading-edge camber on the airfoil pressure distribution.

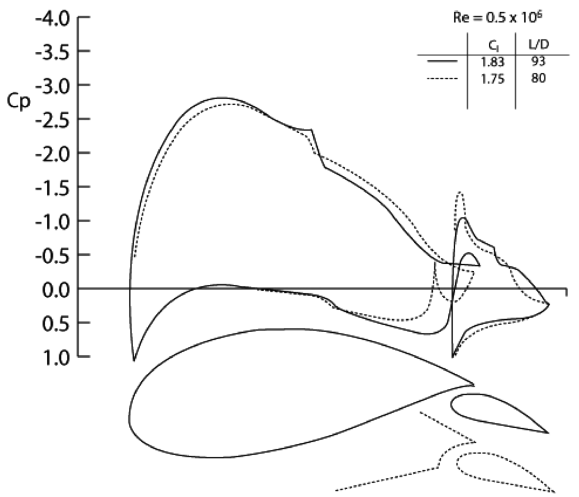

Fig. 5 Effect of flap to main-airfoil gap geometry on pressure distribution.

are presented. Before any computations, however, the chordwise loading from thin airfoil theory may be recalled [Eq. (1)]. Here, the airfoil chord is in the range of $0 < x < c$, and the first term provides some insight into the effect of angle of attack α, whereas the second term shows the effect of camber (for more details on this model and how to evaluate the constant A_1, see [15], pp. 104–106):

$$\Delta C_P = 4\left[\sqrt{\frac{c}{x} - 1}\cdot\alpha + \frac{4x}{c}\left(1 - \frac{x}{c}\right)\cdot A_1\right] \tag{1}$$

The first term clearly demonstrates the effect of angle of attack, which tends to increase the suction peak near the leading edge, whereas the second "sine shape" term shows that a high camber moves the loading more backward. These trends are valuable during the initial iterations and such an example is shown in Fig. 4. Note the effect of a "minor" change in the leading-edge camber and, consequently, the dramatic change in the upper surface pressure distribution. Clearly, drooping the leading edge brings the pressure distribution shape closer to the target set earlier in Fig. 2. Also upper-boundary-layer transition was pushed beyond $x/c > 40\%$, resulting in lower skin friction (and drag) in this region. On the other hand, the transition in the case of the larger leading-edge suction is expected behind the suction peak and, because of the sharp adverse pressure, the flow separates at about the same point on the upper surface ($x/c > 40\%$). The lift coefficient for the drooped-leading-edge airfoil (which is better than the stalled one) is near 1.8 and L/D is about 43; clearly not close to the target values. Based on Fig. 4, improvement can be made by eliminating the main element's trailing-edge flow separation, and by improving the flow in the gap area. Note that the converging–diverging gap accelerates the flow locally, and this portion of the trailing edge actually creates negative lift. The flow over the flap is well behaved and upper surface transition is near 30% of its chord (for brevity, parameters supporting these arguments, such as skin friction or shape factor, are not plotted here).

To correct the aforementioned problem in the gap region, several approaches were tested. The traditional flap-gap, where the flap is a rotating part of a single element airfoil's trailing edge, is shown in Fig. 5 (dashed lines). In this case, the gap is a simple channel energizing the upper boundary layer and it is quite effective in eliminating the previously mentioned negative lift at the main element's trailing edge. However, the flow accelerates around the sharp corner at the front of the gap, resulting in an undesirable suction peak on the main element (with negative contribution to the lift). This gap flow can also be viewed as a local channel flow and it appears to have a negative effect on the flap. The flap upper surface now has a larger suction peak near its leading edge (see Fig. 5), promoting earlier transition and eventual trailing-edge separation (which was not there in the previous iteration). One positive outcome of this change was the reduction of the main element trailing-edge

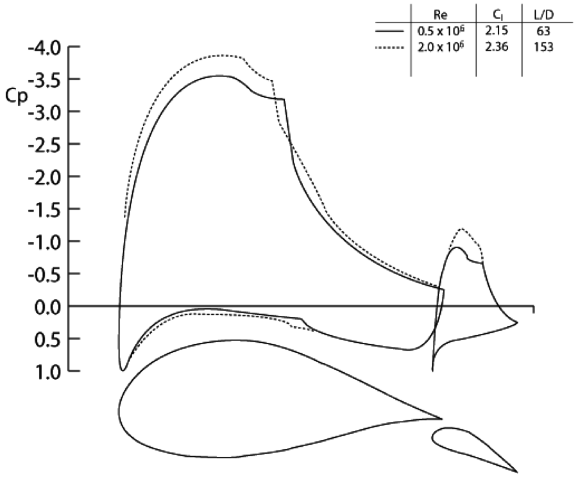

Fig. 6 Effect of Reynolds number on the pressure distribution of the final configuration. ($\alpha = 0$, $\delta = 0$. Note that the $\delta = 0$ and $\alpha = 0$ conditions are defined for the condition as shown in the inset.)

separation, resulting in a significant increase in the computed L/D. Because, for the current application, the flap is not expected to retract into the main airfoil (and so, no geometrical limitations there), the "converging" gap[‡] was used for the final configuration, as shown in Fig. 6.

The design process is considered converged once the targeted pressure distribution on the airfoil and its flap were approached and minor modifications had less than 1% effect on the desirable lift and drag values. At this point, a more detailed map was created by evaluating the lift and drag through a variety of expected angles of attack and flap deflections (actually, this was done for interim designs as well). These calculated lift and drag results are provided later. Reynolds number effects were checked as well, and results for the final configuration are shown in Fig. 6. Also note that this is a high-lift design which is not efficient at lower lift coefficient values. The expected UAV would operate near a constant C_L and, to avoid large negative angles (during takeoff), its lift may be controlled by slower flight speeds (to avoid large angle-of-attack changes).

Returning to Fig. 6, it becomes clear that, at the higher Reynolds numbers, both lift and drag values improve. Although transition moved a bit forward (for the higher Re number), both on the upper and lower surfaces, boundary-layer thickness near the trailing edge

[‡]A converging gap is when the clearance between the two airfoil elements is gradually decreasing toward the upper surface exit.

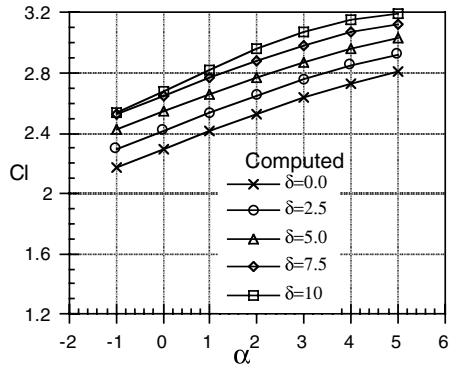

Fig. 7 Computed lift coefficient results vs angle of attack and flap deflection for the final airfoil shape ($Re = 1.0 \times 10^6$).

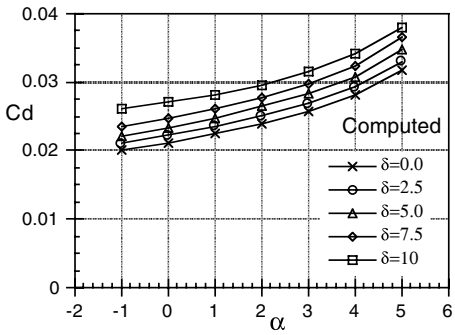

Fig. 8 Computed drag coefficient results vs angle of attack and flap deflection for the final airfoil shape ($Re = 1.0 \times 10^6$).

was reduced, resulting in more circulation (in terms of ideal flow). Also note that the flap at this condition is not heavily loaded (and so, more flap angle δ can be used).

Calculated Lift and Drag Results

The thickness ratio of the final airfoil shape depicted in Fig. 6 was close to 24.5%, which is beyond the initially set target. The large leading-edge radius was desirable to fit a fuel tank there, and the highly cambered upper surface was dictated by the need for high lift. Once the airfoil geometry was finalized, its aerodynamic performance was calculated for a range of flap deflections and angles of attack. A summary of the computed lift and drag coefficient data for the airfoil shape of Fig. 6 is presented in Figs. 7 and 8. Although the Reynolds number range evaluated numerically was between 0.5×10^6 and 2.0×10^6 (as suggested by Fig. 6), only the data for $Re = 1.0 \times 10^6$ are presented in Figs. 7 and 8 (and, as noted, the effect of Re number on the computed results was small). Because of the high upper surface curvature of this airfoil, its angle-of-attack range is limited to the range between $\alpha = -1$ and 5 deg (although in , it was experimentally checked up to $\alpha = 7$ deg). The data in Fig. 7 suggest that lift coefficient values beyond two are possible with this design, and there is no stall within the shown angle-of-attack range (as long as $Re > 0.6 \times 10^6$).[§] These high-lift calculations were validated in a wind-tunnel test and results are presented in [16]. However, due to three-dimensional effects in those tests, the drag data in Fig. 8 were not satisfactorily validated. Because of the large size of an expected UAV using such an airfoil, the angle of attack will not change much (beyond $\alpha = 0$), and lift control can be achieved by using flap deflections δ. The calculations show that, even at $\delta = 7.5$ deg, there is an almost linear lift increment; however, beyond this large deflection, the flap stalls. It must be pointed out that the range of performance, however, is limited to the range shown in Fig. 7 and a $C_l = 0.6$, for example, cannot be efficiently obtained (because of the highly cambered shape).

The calculated drag coefficient data for the same conditions (of Fig. 7) are presented in Fig. 8. Again, for the smaller flap deflection, the drag increment is smaller than for the $\delta = 10$ case. This is a result of flow separation on the flap, which was predicted by the calculations. Near the expected cruise condition ($\alpha = 0$ deg), however, the drag is fairly low, even with flap deflection of $\delta = 5$ deg. Consequently, this simulation provided encouraging indications that two-dimensional section lift-to-drag ratios near 70 are possible. However, further large-aspect-ratio tests are required to validate the functionality of such a thick and high-lift airfoil shape for an actual three-dimensional wing (because this case may be outside the envelope of the method presented in [14]).

[§]Although the planned Reynolds number range was above $Re = 0.5 \times 10^6$, tests in [16] validated the performance only above $Re > 0.6 \times 10^6$

Conclusions

A high-lift airfoil was developed for high-altitude UAV applications. The added thickness allows the design of a stiffer structure (with less spanwise bending) and with increased internal volume. The calculations indicate that, in spite of the extreme thickness, very high-lift coefficients are possible without compromising lift-to-drag ratio (e.g., an L/D of about 70 is possible for $Re > 0.6 \times 10^6$). Based on the current study, an optimization algorithm may be developed to achieve faster and more efficient results. Because of the highly cambered upper surface, the lift coefficient and angle-of-attack range is limited to high-lift conditions only. Consequently, such an airfoil cannot operate at a lower lift coefficient (e.g., at $C_l < 0.6$).

References

[1] Romeo, G., Frulla, G., Cestino, E., and Corsino, G., "HELIPLAT: Design, Aerodynamic and Structural Analysis of Very-Long Endurance Solar Powered Stratospheric UAV," *Journal of Aircraft*, Vol. 41, No. 6, 2004, pp. 1505–1520. doi:10.2514/1.2723

[2] Romeo, G., and Frulla, G., "HELIPLAT: High Altitude Very-Long Endurance Solar Powered UAV for Telecommunication and Earth Observation Applications," *The Aeronautical Journal*, Vol. 108, No. 1084, 2004, pp. 277–293.

[3] Hicks, R. M., and Schairer, E. T., "Effects of Upper Surface Modification on the Aerodynamic Characteristics of the NACA 632-215 Airfoil Section," NASA TM-78503, 1979.

[4] McGhee, R. J., and Beasley, W. D., "Wind-Tunnel Results for a Modified 17-Percent-Thick Low-Speed Airfoil Section," NACA Technical Paper 1919, 1981.

[5] Koss, D., Steinbuch, M., and Shepshelovich, M., "Development of Two-Element NLF Airfoils for Long Endurance Flight," *35th Aerospace Meeting*, AIAA Paper 97-0514, Jan. 1997.

[6] Steinbuch, M., Marcus, B., and Shepshelovich, M., "Development of UAV Wings: Subsonic Designs," *41st Aerospace Sciences Meeting*, AIAA Paper 2003-603, Jan. 2003.

[7] Steinbuch, M., and Shepshelovich, M., "Development of High Altitude Long Endurance Airfoils," *42nd Aerospace Sciences Meeting*, AIAA Paper 2004-1052, Jan. 2004.

[8] Biber, K., and Ol, M. V., "Some Examples of Airfoil Design for Future Unmanned Air Vehicle Concepts," *42nd Aerospace Sciences Meeting.*, AIAA Paper 2004-1050, Jan. 2004.

[9] Biber, K., and Tilmann, C. P., "Supercritical Airfoil Design for Future High-Altitude Long-Endurance Concepts," *Journal of Aircraft*, Vol. 41, No. 1, 2004, pp. 156–164. doi:10.2514/1.1049

[10] Somers, D. M., and Tangler, J. L., "Wind-Tunnel Test of the S814 Thick-Root Airfoil," *Proceedings of the American Society of Mechanical Engineers*, Vol. 16, American Society of Mechanical Engineers, Solar Energy Div., Fairfield, NJ, 1995, pp. 137–141.

[11] Liebeck, R. H., "Class of Airfoils Designed for High Lift in Incompressible Flow," *Journal of Aircraft*, Vol. 10, No. 10, 1973, pp. 610–617. doi:10.2514/3.60268

[12] Liebeck, R. H., "Design of Subsonic Airfoils for High Lift," *Journal of Aircraft*, Vol. 15, No. 9, 1978, pp. 547–561. doi:10.2514/3.58406

[13] Drela, M., "Elements of Airfoil Design Methodology," *Applied Computational Aerodynamics*, Vol. 125, Progress in Astronautics and Aeronautics, AIAA, Washington, D.C., 1990, pp. 167–190.

[14] Drela, M., "User's Guide to MSES 2.8," Ver. 2.8, Massachusetts Inst. of Technology, Dept. of Aeronautics and Astronautics, Cambridge, MA, May 1995.

[15] Katz, J., and Plotkin, A., *Low-Speed Aerodynamics*, 2nd ed., Cambridge Univ. Press, New York, 2001.

[16] Cerra, D., and Katz, J., "Design and Evaluation of a High-Lift, Thick Airfoil for UAV Applications," AIAA Paper 2008-0292, Jan. 2008.